Int J Fract
DOI 10.1007/s10704-010-9475-8

ORIGINAL PAPER

Dynamic failure by adiabatic shear banding

D. Rittel · S. Osovski

Received: 29 October 2009 / Accepted: 8 March 2010
© Springer Science+Business Media B.V. 2010

Abstract This paper addresses adiabatic shear localization from a different point of view. New results are reviewed which indicate that the process can be viewed as triggered by dynamic recrystallization instead of being the result of thermal softening as universally assumed. A simple dislocation dynamics model (modified ETMB) is used to reproduce the salient features of the physical observations, namely dynamic recrystallization in the strain-hardening phase with a minor temperature rise. The main parameters of the model are discussed from an experimental identification point of view.

Keywords Adiabatic shear localization · Dislocation dynamics · Dynamic recrystallization

1 Introduction

Dynamic failure of solids may occur by brittle fragmentation or following a certain amount of plastic deformation, whose values depend on the material in question. The plastic deformation will usually proceed homogeneously at first, but at a certain stage, it may tend lo localize. Localization means that the plastic deformation will concentrate into a given plane into which the strains may reach extremely large values by comparison with the surroundings. The exact geometrical shape of the plane of localization varies with the geometry of the structure, being conical for a dynamically deformed cylindrical specimen or simply planar when located at the tip of a crack. Long ago, Tresca (1879) observed the formation of a glowing X-like sign on forged billets of platinum, and he attributed this phenomenon to a localized intense conversion of the mechanical energy into heat. The concept of thermomechanical coupling through which part of the energy invested in the plastic deformation process turns into heat under certain conditions was thoroughly investigated by Farren and Taylor (1925), and Taylor and Quinney (1934). The thermomechanical conversion mechanisms was later identified by Zener and Hollomon (1944) as the primary factor responsible for the gradual material softening, leading ultimately to the loss of stability of plastic deformation and formation of a localized band (plane). Such a plane is usually referred to as an adiabatic shear band or ASB (Bai and Dodd 1992) to express the fact that in view of the temporal and spatial scales involved, heat conduction can be neglected to a first approximation (Boley and Weiner 1960), so that the process is viewed as adiabatic. The term "shear" here refers to the fact that shear localization consists of an intense shear strain in the band itself, while the actual band width requires some heat transfer to operate (Merzer 1982). Coincidentally with the adiabatic shear band, a very significant temperature rise can be observed, of the order of several hundred degrees (Hartley et al. 1987).

D. Rittel (✉) · S. Osovski
Faculty of Mechanical Engineering, Technion,
32000 Haifa, Israel
e-mail: merittel@technion.ac.il

Published online: 25 March 2010

These observations and physical models are very well accepted today, and almost every single paper on adiabatic shear localization mentions a measured, calculated or modeled intense temperature rise in the shear band with the prevailing assumption that this temperature rise actually led to the onset of the phenomenon, in the spirit of Zener and Hollomon (1944).

The purpose of this paper is to question these assumptions based on several measurements carried out by the authors, while exposing a different physical picture for which a preliminary model is proposed.

Therefore, the main points to be addressed in this paper are the following:

1. Is the thermal softening model universal?
2. Is there another physical mechanism?
3. How to link mechanical and microstructural observations in a coherent way?
4. A preliminary model for the onset of ASB formation.

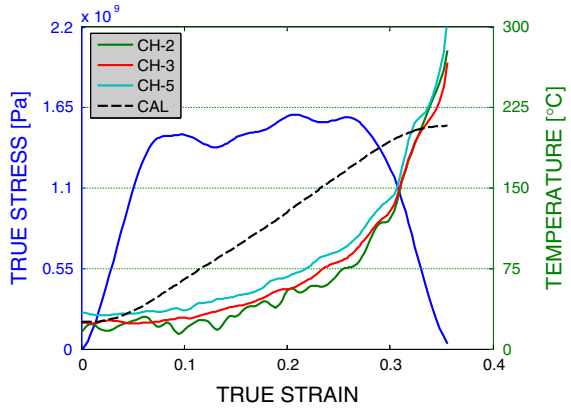

Fig. 1 Typical stress and temperature vs. strain for an impacted Ti6Al4V alloy. The temperature is measured on three channels and calculated (*dashed line*) according to $\beta_{\text{int}} = 1$. Note that the measured temperature rise is quite modest during most of the deformation process, including the peak stress from which a shear band might be thought to be fully formed. The measured temperature rise is also significantly smaller that the one that is calculated using a full thermomechanical conversion. (Reprinted after Rittel and Wang 2008)

2 Some remarks on the adiabatic shear process

As stated in the introductory section, the first point to be addressed is that of the universality of a thermal softening process leading to adiabatic shear band formation. Here one must first remark that in the (nearly) adiabatic process, heat is generated in the deforming solid as a result of the conversion of mechanical energy into heat, a thermodynamical process with a given efficiency denoted by β_{int}, as follows:

$$\beta_{\text{int}} \int_0^{\varepsilon_p} \sigma_{ij} \dot{\varepsilon}_{ij}^p \mathrm{d}t = \rho C_p \Delta T \tag{2.1}$$

where σ and ε are the components of the stress and plastic strain tensors, respectively, ρ is the material density, C_p the heat capacity and ΔT is the temperature rise. Here, a common assumption is made that $\beta_{\text{int}} = 0.9$, following Taylor and Quinney (1934). However, this assumption appears to be an upper bound, namely when experimental work on metals and polymers indicates that β_{int} is not a constant, but rather a property that is both strain and strain-rate dependent (Hodowany et al. 2000; Rittel 1999). From an experimental point of view, when one looks at earlier work on real-time measurements during the adiabatic shear process (Duffy and Chi 1992; Hartley et al. 1987; Liao and Duffy 1998; Marchand and Duffy 1988), it clearly appears that the overall temperature rise in the gauge section prior to localization is quite modest. As an illustration, Fig. 1, shows the measured temperature rise in a Ti6Al4V specimen, deformed at a high strain rate, as recorded by a linear array of infrared detectors with a spatial resolution of $45 \times 45 \mu$m (Rittel and Wang 2008). Note that, if the localization process is assumed to start with the stress drop ($\varepsilon \approx 0.27$), the stress-strain curve is representative of a homogeneous adiabatic response. However, this assumption is based on macroscopic considerations whereas, as shown in the sequel, considerable microstructural rearrangements have occurred until that point which are deemed to affect the strain homogeneity in the specimen.

Setting aside temporarily the issue of β_{int}, one should realize that materials could tentatively be divided into two categories: high strength-limited ductility to failure (e.g. Ti alloys, maraging steels), or low strength-high ductility to failure (plain carbon steels and non ferrous metals). While strength and ductility to failure are usually not simultaneously high in a given material, these two parameters nevertheless govern the amount of strain energy causing the temperature rise. This physical observation casts a doubt on the universality of a thermally induced loss of stability leading to shear localization. One can indeed argue that the thermal measurements are made with a given spatial (temporal)

resolution below which very small spots of heat could be generated. To get a physical picture of this possibility, one may solve the transient heat equation for a 1 mm medium whose edges are kept to a constant temperature of 300 K, while a 45 μm long source is placed at half-length with an initial temperature of 800 K. This evaluation, suggested by V. Nesterenko (Personal communication, 2009), shows that for commercial titanium, the temperature of the source will decay within about 1 ns. For a much lower conductive polycarbonate, the process will take about 100 ns, due to the linearity of the problem with respect for the heat conductivity. If the medium is made shorter, heat will be evacuated at a higher rate. This back of the envelope calculation suggests that if a hot spot develops with a typical size that is inferior to the thermal detector's pixel (which is also that of a typical metal grain), this thermal source will decay in a very short time that is much too short to significantly affect the material. Consequently, a first conclusion is that within the experimental limits of the thermal measurement system, the average temperature of the gauge section of the specimen experiences a rather modest temperature rise for most materials which is unlikely to cause a significant softening. In parallel, the eventuality of the development of very small spots seems unlikely as their lifetime is necessarily limited as they get quenched by the colder surroundings. Consequently, one has to look for a different physical mechanism that would cause a loss of material stability through local softening.

A series of experiments were recently carried out in order to investigate the notion of a critical strain for adiabatic shear banding (Rittel et al. 2006). In these experiments, specimens were subjected to quasi-static straining, followed by impact to fracture tests. The outcome of these experiments was that one quantity remains constant and un-affected by the quasi-static preloading phase, namely the deformation (strain) energy invested in the subsequent dynamic phase only. When this observation is coupled to the observed lack of thermal softening in the experiments, one can conclude that the stored energy of cold work (Bever et al. 1973) is in fact the relevant factor for the shear localization process. This conclusion is reached by considering the partition of strain energy into thermal and stored energy, noting that the thermal part is of little influence. This new approach to adiabatic shear localization is interesting in the sense that it ties a global mechanical concept (energy) to the microstructure of the material since the stored energy is directly related to the density and configuration of defects such as dislocations. In that respect, this observation opens a new way of bridging mechanical and microstructural aspects of the problem in a way that was not suggested in previous studies.

Having identified the stored energy as related, or perhaps as the driving force for localization, the next logical step is to identify those microstructural factors that are on the one hand representative of adiabatic shear localization and are likely to trigger it on the other hand. Here, one must note a quasi-universal observation for all the metallic materials that failed by ASB, namely the observation of an increasingly refined microstructure all the way to the formation of dynamically recrystallized grains (DRX) in the band itself (Andrade et al. 1994; Meyers 1994; Meyers et al. 2000). Yet, another universal claim is that DRX develops in those heavily sheared sections that have reached very high temperatures due to the localization process. In other words, DRX is considered as the outcome of dynamic shear localization. To investigate this point, Rittel et al. (2008) carried experiments on a annealed Ti6Al4V for which the propensity to ASB failure is well documented. Some specimens were loaded until failure in a well defined stress-concentration area of the specimen, while a couple of others were loaded until half this failure strain (interrupted tests). For interrupted tests, the stress-strain curve of the material was still in its hardening phase while the average temperature rise was quite negligible. Transmission electron microscopy specimens were prepared from the ASB of the failed specimens and of the stress concentration area of the interrupted specimens. To summarize the main outcome of this work, a striking observation was that the two resulting microstructures were qualitatively identical, showing in both cases the presence of very small dynamically recrystallized grains. These grains were also observed to contain a low density of dislocations. This surprising observation showed that DRX can actually form well before the localization band which can be rationalized if one considers the phenomenon as athermal grain refinement (Hines and Vecchio 1997). One can now tie this observation to the stored energy of cold work by postulating that the latter is the thermodynamic driving force for DRX. Furthermore, one may propose that the formation and the multiplication of these soft nanograins affects (softens) the local stress distribution in the gage section, to a point where a global material instability is observed.

In the next section, we will present a preliminary dislocation-based model whose goal is to describe the evolution of the initially uniform dislocations into cells, while monitoring the misorientation that develops, ultimately resulting in recrystallized grains.

3 Modeling dynamic recrystallization

Dislocation dynamics is a convenient way to represent the microstructural evolution during the development of plastic straining. We will present and discuss a preliminary model based on dislocation dynamics concepts, whose main goal is to qualitatively reproduce some of the physical observations mentioned in the first part of the paper while outlining the influence and importance of each physical parameter that enters the model. The basic microstructural evolution to be addressed here is that of dislocation cells formation and evolution into dynamically recrystallized grains. Two options are considered, namely athermal and adiabatic deformation processes, whose influence is studied separately.

Following the work of Heidenreich and Shockley (1948) we consider the formation of dislocation walls as the polygonization process of an initially uniform distribution of dislocations.

3.1 Phase 1: evolution of the uniform dislocation density

At the beginning of the plastic deformation, mobile dislocations are created to accommodate for the deformation. These dislocations are trapped either by interlocking with other dislocations in the grain or by reaching the grain boundary (sink role only). Thus, integrating Orowan's equation (1948) over time we get:

$$\rho_{\text{tot}}(\varepsilon) = \rho_0 + \rho^+(\varepsilon) \tag{3.1a}$$

$$\rho^+(\varepsilon) = \frac{\varepsilon}{bL_{\text{eff}}}; \quad L_{\text{eff}} = \left(\frac{1}{D} + \frac{1}{\sqrt{\rho_{\text{tot}}}}\right)^{-1} \tag{3.1b}$$

ρ^+ is the increase in the dislocation density for a given strain, D is half the grain size, L_{eff}-the mean free path for dislocations motion, b the magnitude of Burger's vector, ρ_{tot} the total dislocation density, and ρ_0 the initial dislocation density of the unstrained material.

With the ongoing deformation, the dislocation density keeps growing until, at some point, an ordered structure consisting of dislocation cell walls is created.

To estimate the critical density for the above mentioned transition, we compare the strain energy of the two configurations (uniform distribution versus structured dislocation pattern).

The strain energies per unit volume of the two configurations is given in the following set of equations, when E_{uniform} is the energy for the uniformly distributed dislocation density and E_{wall} is the energy for dislocations which are organized into dense dislocation walls surrounding a dislocation-free cell.

$$E_{\text{uniform}} = \rho_{\text{tot}}\left(\frac{AGb^2}{4\pi}\right)\ln\left(\frac{\alpha}{2b\sqrt{\rho_{\text{tot}}}}\right) \tag{3.2a}$$

$$E_{\text{wall}} = \rho_{\text{tot}}\left(\frac{AGb^2}{4\pi}\right)\ln\left(\frac{e\alpha}{4\pi b}\frac{S}{V}\frac{1}{\rho_{\text{tot}}}\right) \tag{3.2b}$$

where G stands for the shear modulus, A is a constant depending on the character of dislocation (screw or edge), and α a constant of the order of 0.5 related to the core energy of the dislocation, while S and V stand for the surface and volume of the cell, respectively, (Hirth and Lothe 1968; Meyers et al. 1996).

When the dislocation density ρ_{tot} is such that the strain energy given in Eq. 3.2a is higher than that of a cell structure (Eq. 3.2b), the dislocations will start to polygonize. From this criterion we get the critical dislocation density (ρ_{crit}) at which the newly structured phase is more stable.

To account for the kinetics of this process, we assumed that once the critical density was reached, the dislocations which are still uniformly distributed will start to evolve toward the creation of dislocations cells and walls. Here, we will use evolution equations that describe a fully formed structure (Estrin et al. 1998). In other words, the dislocations at that point are regarded as a very diffused wall surrounding a smaller area which will grow to be the dislocation cell as the wall gets sharper, as discussed in the sequel.

3.2 Phase 2: dislocation cells and walls

To describe the evolution of the dislocations once the density has reached its critical value, we use the Estrin–Toth–Molinari–Bréchet (ETMB) dislocation model (Estrin et al. 1998; Estrin et al. 2006)

The ETMB model assumes that the microstructure can be decomposed into two phases: the dislocation walls (hard phase) with dislocation density ρ_{wall} and the other, softer phase, being the dislocation cell with ρ_{cell}. The total dislocation density is then given by a rule of mixture:

$$\rho_{\text{tot}} = f\rho_{\text{wall}} + (1-f)\rho_{\text{cell}} \tag{3.3a}$$

$$f = f_\infty + (f_0 - f_\infty)\exp\left(-\frac{\gamma}{\gamma_0}\right) \tag{3.3b}$$

f being the volume fraction of the wall phase, γ_0 the shear strain, γ_0 a decay parameter, f_0 and f_∞ the initial and saturated volume fraction of the wall phase. The transition between phase 1 (uniform distribution of dislocations) to phase 2 (structured dislocations pattern), is done by taking f_0 to be close to 1, thus claiming that the uniformly distributed dislocations are forming into a dense dislocation wall getting sharper as the value of f decreases according to Eq. 3.3b.

The evolution equation for the two populations of dislocation (ρ_{wall} and ρ_{cell}) is given in Eq. 5 (Estrin et al. 1998):

$$\dot{\rho}_{\text{cell}} = \alpha^* \frac{2}{3\sqrt{3}} \frac{\sqrt{\rho_{\text{wall}}}}{b}\dot{\gamma}_w - \beta^* \frac{6\dot{\gamma}_c}{bd\sqrt{1-f}} - k_{0c}\left(\frac{\dot{\gamma}_c}{\dot{\gamma}_{0,r}}\right)^{\frac{-1}{n_c}} \dot{\gamma}_c \rho_{\text{cell}} \tag{3.4a}$$

$$\dot{\rho}_{\text{wall}} = \frac{6\beta^*\dot{\gamma}_c\sqrt{1-f}}{bdf} + \frac{2\beta^*\dot{\gamma}_c(1-f)\sqrt{\rho_{\text{wall}}}}{fb\sqrt{3}} - k_{0w}\left(\frac{\dot{\gamma}_w}{\dot{\gamma}_{0,r}}\right)^{\frac{-1}{n_w}} \dot{\gamma}_w \rho_{\text{wall}} \tag{3.4b}$$

where:

α^*, β^*—numerical constants related to the fraction of operative Frank-Read sources in the cell and walls, respectively,
f—volume fraction of walls
$\dot{\gamma}_c$, $\dot{\gamma}_w$—shear strain rate in the cell and walls, respectively
$\dot{\gamma}_{0,r}$—a reference shear strain rate
d—cell size
k_{0c}, k_{0w}—recovery term constants in cell and wall, respectively
n_i—recovery exponents expressed as $n_i = \frac{B_i}{T}$
B_i—material constants

The cell size d is given by Eq. 3.5 with K being a proportionality constant (Kubin 1993) :

$$d = \frac{K}{\sqrt{\rho_{\text{tot}}}} \tag{3.5}$$

In the original ETMB model, the recovery terms in Eq. 5 (third term in the rhs of Eq. 5) are identical for the cell and wall phase. While the recovery in the walls is mostly done by cross-slip process for which the constant B_i is taken to be the melting temperature, the recovery in the cells is thought of as more complex, being the result of combined mechanisms such as dipole–dipole interactions and climb at the higher temperatures. To account for the difference in recovery mechanisms, we took the recovery constants in the cell to be different then those in the wall (Hosseini and Kazeminezhad 2009), and thereby less sensitive to temperature than in the walls.

Having defined the dislocations populations and their evolution equations, the resulting stress can be calculated using the following set of equations (Estrin et al. 2006; Kocks 1976):

$$\tau = f\tau_w + (1-f)\,\tau_c \tag{3.6a}$$

$$\tau_w = \tau_0^w \left(\frac{\dot{\gamma}_w}{\dot{\gamma}_0}\right)^{\frac{T}{Tm}} \quad ; \tau_0^w = \alpha G b\sqrt{\rho_{\text{wall}}} \tag{3.6b}$$

$$\tau_c = \tau_0^c \left(\frac{\dot{\gamma}_c}{\dot{\gamma}_0}\right)^{\frac{T}{Tm}} \quad ; \tau_0^c = \alpha G b\sqrt{\rho_{\text{cell}}} \tag{3.6c}$$

where τ_c, and τ_w are the shear strain and stress in the cells and walls, τ the total shear stress, $\dot{\gamma}_c$, $\dot{\gamma}_w$ are the shear strain rate in the cells and walls, respectively, both of which are taken equal to the total shear strain rate, α is a constant of the order of 0.5. Tm is the melting temperature and $\dot{\gamma}_0$ a reference shear strain rate. The effective stress is then given by Eq. 3.7 with M being the Taylor factor (Nes 1998).

$$\sigma = \sigma_0 + \alpha M \tau \tag{3.7}$$

Estrin et al. (2006) introduced into the ETMB model the accumulation of geometrically necessary dislocations (GND's). The evolution equation for the GND's, which completes and modifies Eq. 5, is given by :

$$\dot{\rho}_{\text{GND}} = \xi \frac{6\beta^*\dot{\gamma}_c\,(1-f)^{2/3}}{bdf} \tag{3.8}$$

When ξ is the fraction of incoming dislocation from the cell interior that lead to the misorientation, a concept that will be needed to define dynamic recrystallization. Equation 5 is then modified to the following:

$$\dot{\rho}_{\text{cell}} = \alpha^* \frac{2}{3\sqrt{3}} \frac{\sqrt{\rho_{\text{wall}} + \rho_{\text{GND}}}}{b} \dot{\gamma}_w - \beta^* \frac{6\dot{\gamma}_c}{bd\sqrt{1-f}} - k_{0c} \left(\frac{\dot{\gamma}_c}{\dot{\gamma}_{0,r}} \right)^{\frac{-1}{n_c}} \dot{\gamma}_c \rho_{\text{cell}} \tag{3.9a}$$

$$\dot{\rho}_{\text{wall}} = (1-\xi) \frac{6\beta^* \dot{\gamma}_c \sqrt{1-f}}{bdf} + \frac{2\beta^* \dot{\gamma}_c (1-f)\sqrt{\rho_{\text{wall}} + \rho_{\text{GND}}}}{fb\sqrt{3}} - k_{0w} \left(\frac{\dot{\gamma}_w}{\dot{\gamma}_{0,r}} \right)^{\frac{-1}{n_w}} \dot{\gamma}_w \rho_{\text{wall}} \tag{3.9b}$$

And the total dislocations density ρ_{tot} is given by:

$$\rho_{\text{tot}} = f(\rho_{\text{wall}} + \rho_{\text{GND}}) + (1-f)\rho_{\text{cell}} \tag{3.10}$$

From Eq. 3.8 it follows that as the strain increases the cells/subgrains accumulate more and more GND's, thus enhancing the misorientation angle between neighboring cells. Since the expression given in Eq. 3.8 has no loss terms, even after saturation of stress, the value of the GND density and thus the misorientation angle will keep increasing without bounds. This does not account for the fact that once the cell has rotated to a certain angle, it certainly needs much less GND's as strain incompatibility has been reduced.

To overcome this issue, we introduced an angle (θ) dependent ξ of the following form :

$$\xi = \xi_0 \exp(-\frac{\theta}{\theta_0}) \tag{3.11}$$

The misorientation angle between two neighboring cells can be calculated by (Estrin et al. 2006):

$$\theta = a \tan\left(b\sqrt{\rho_{\text{GND}}}\right) \approx b\sqrt{\rho_{\text{GND}}} \tag{3.12}$$

At this stage, a short discussion on the model parameters is required. The ETMB model is a constitutive model which is based on real physical phenomena. Therefore, we sought a way to choose the model parameters not only by fitting the calculated stress-strain curve to a measured one, but by using a set of microstructural properties which can be obtained experimentally as well. One of the readily obtainable quantities from experiments is the saturation value of the subgrain size. This value in the model is strongly related to two parameters: K, and the wall dislocation density (ρ_{wall}), which in turn is strongly dominated by β^*. By taking Eqs. 3.9a and 3.9b to be equal to zero, assuming that all the other strain dependent parameters such as misorientation and the volume fraction of the walls (f), have saturated as well, we obtain the following set of equations:

$$\frac{6\beta^*(1-f_0)^{2/3}}{f_0 K b}\sqrt{\rho_{\text{tot}}} + \frac{\sqrt{3}\beta^*(1-f_0)}{bf_0}\sqrt{\rho_{\text{wall}}} - k_w \rho_{\text{wall}} \left(\frac{\dot{\gamma}}{\dot{\gamma}_0}\right)^{-T/\text{Tm}} = 0 \tag{3.13a}$$

$$\frac{\alpha^*}{\sqrt{3}b}\sqrt{\rho_{\text{wall}}} - \frac{6\beta^*}{bK(1-f_0)^{1/3}}\sqrt{\rho_{\text{tot}}} - k_c \rho_{\text{cell}} \left(\frac{\dot{\gamma}}{\dot{\gamma}_0}\right)^{-T/B_c} = 0 \tag{3.13b}$$

Assuming the dislocations density in the wall and cell interior can be measured at their saturation values or close to them, along with the values of the average misorientation angle, and calculating the temperature using Eq. 2.1, one can solve Eqs. 3.13a, 3.13b and Eq. 3.12 to obtain sets of parameters related to a given microstructure.

The fitting procedure should be done very carefully, keeping in mind that since the model parameters are strongly related to microstructural parameters, a set of parameters predicting the stress-strain curve satisfactorily but not complying with other measured microstructural quantities is invalid. For example, by adjusting the ratio between α^* and β^*, one easily gets two sets of parameters with which a nice fit to a measured stress-strained is obtained, but one of them will exhibit a larger dislocation density in the grain interior then in the walls, which is unphysical!

Another significant parameter in the model, especially when used to determine the point at which a cell transforms into a DRXed subgrain is the parameter ξ introduced in Eq. 3.8. This parameter controls the rate at which the misorientation angle increases. The physical meaning of ξ is the amount of GND entering the walls. Without considering a specific material, we tested values in the range of up to 0–0.1 which accounts for up to 10% of the incoming dislocations. This parameter, however, can be easily determined given the average misorientation angle at two or more strains, as measured from experiments.

All the model parameters, are summarized in Table 1. They were not calibrated to a specific metal, but set such as to show the general picture described in the previous section, while keeping to the same order of magnitude as those used for this model in other works

Table 1 Model parameters

Parameter description	Nomenclature	Selected value	References
Fraction of active sources in cell interior	α^*	0.08	0.0024–0.065
Fraction of active sources in wall interior	β^*	0.18	0.0054–0.062
Melting temperature [K]	Tm	1,360	
Reference shear strain rate [s^{-1}]	$\dot{\gamma}_0$	1×10^4	1
Reference shear strain rate [s^{-1}]	$\dot{\gamma}_{0,r}$	1×10^6	1
Magnitude of burger's vector [m]	b	2.56×10^{-10}	2.56×10^{-10}
Saturated volume fraction of the walls	f_∞	0.06	0.06
Sharpening rate of the walls	γ_0	1.0	2.0–3.2
Proportionality constant for the cell size	K	23	10–25
Taylor factor	M	2.05	–
Recovery constant for the walls	K_{0w}	1.6	1.4–9.2
Recovery constant for the cells	K_{0c}	2.3	1.4–9.2
Recovery exponent for the cells [K^{-1}]	B_c	14×10^3	15000–20100
Decay rate of increase in GND's [degrees]	θ_c	10	NA
Initial value for the volume fraction of GND's in the walls	ξ	0.1	NA

The reference values are from (Estrin et al. 2006; Hosseini and Kazeminezhad 2009)

(Estrin et al. 1998; Estrin et al. 2006; Hosseini and Kazeminezhad 2009).

4 Results of the simulation

Using the parameters given in Table 1, we calculated the evolution of the microstructure of a single grain being strained at a constant strain rate of $\dot{\varepsilon} = 3 \times 10^3\ s^{-1}$, and compared the athermal and adiabatic deformation processes. The temperature was calculated using Eq. 2.1 taking β_{int}=1. A calculated stress-strain curve, for the two cases, is shown in Fig. 2 We also indicated the strain at which the grain starts to undergo dynamic recrystallization, defined to start at $\theta \geq 3°$, corresponding to $\varepsilon = 0.42$.

Figure 2 clearly shows that the DRX'ed grains appear during the hardening stage both for both the thermal and athermal cases. It is also noted that the temperature at which DRX starts (Fig. 3) is of the order of 0.3 Tm which rules out thermal activation. These results are qualitatively in good agreement with the physical characteristics of DRX and the related ASB, namely development of DRX during the strain-hardening phase with a negligible temperature rise. As stated in the introduction, it is believed that early DRX favors shear localization through the growth and coalescence of soft DRX'ed islands, as proposed by Rittel et al. (2008).

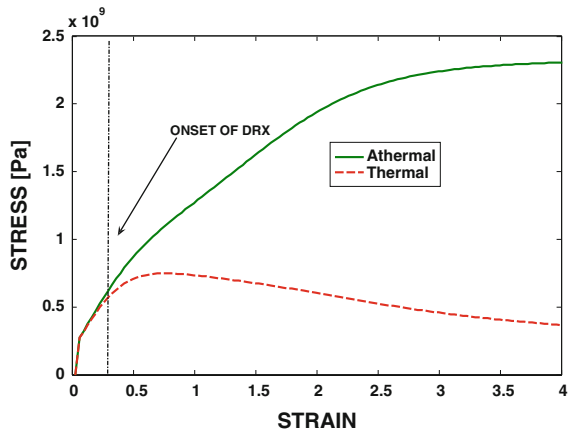

Fig. 2 Calculated stress-strain curve for one grain being strained at a strain rate of $2 \times 10^3\ s^{-1}$, for both thermal and athermal cases

Considering now the thermally coupled calculation, it appears that the evolution of heat, while not affecting the DRX process, actually limits the maximum stress attainable, but most of all induces a strain-softening phase beyond peak stress which is always observed experimentally. In other words, while thermally activated processes, as modeled here, do not affect the basic physics of the DRX, they certainly intervene at the later stages of the deformation process in the form of thermal softening, a stage at which the adiabatic shear band is obviously well developed.

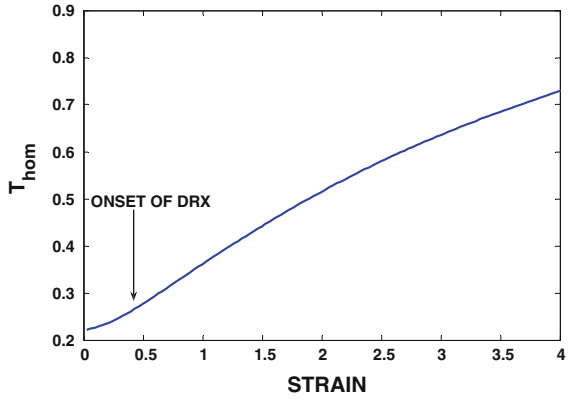

Fig. 3 Calculated evolution of the homologous temperature

5 Discussion and conclusion

This paper is divided in two parts. The first part presented new evidence on the genesis of adiabatic shear band formation, which is interpreted as a microstructural mechanical transformation (DRX) for which thermally activated processes are obviously of a minor importance in the investigated cases. The second stage which is the logical continuation of the first presents the application of a simple modified model for the microstructural evolution. This model, based on dislocation dynamics, contains many adjustable parameters whose choice is crucial for the calculated results. Here, we used most of the constants reported in the literature, but in parallel we discussed how several of these constants can be identified experimentally (mostly through transmission electron microscopy). The outcome of the simulations was qualitatively similar to the physical observations, in the sense that DRX which precedes shear localization was shown to occur without a significant thermal activity, gradually during the strain-hardening phase, which seems to rule out a brutal instability as previously thought of. While the model is still preliminary and considers only one grain, it can now be extended to investigate the two dimensional case for which the initial dislocation distribution, and probably other parameters, are statistical in nature, so that the quantitative and spatial evolution of the DRX can be characterized, thus providing essential guidelines for future microstructural characterization.

To conclude, a simple dislocation dynamics model was proposed whose outcome is the correct reproduction of an identified trend for the onset of DRX during the strain-hardening stage for which thermally activated processes are of minor importance.

Acknowledgments The support of Israel Science Foundation (grant 2011362) is kindly acknowledged.

References

Andrade U, Meyers MA, Vecchio KS, Chokshi AH (1994) Dynamic recrystallization in high strain, high strain rate plastic deformation of copper. Acta Metall Mater 42:3183–3195

Bai Y, Dodd B (1992) Shear localization: occurrence, theories, and applications. Pergamon, Oxford

Bever M, Holt D, Titchener A (1973) The stored energy of cold work. Pergamon, London

Boley BA, Weiner JH (1960) Theory of thermal stresses. Wiley, New York

Duffy J, Chi Y (1992) On the measurement of local strain and temperature during the formation of adiabatic shear bands. Mater Sci Eng A 157:195–210

Estrin Y, Toth L, Molinari A, Brechet Y (1998) A dislocation-based model for all hardening stages in large strain deformation. Acta Mater 46:5509–5522

Estrin Y, Tóth LS, Bréchet Y, Kim HS (2006) Modelling of the evolution of dislocation cell misorientation under severe plastic deformation. Mater Sci Forum 503(504):675–680

Farren WS, Taylor GI (1925) The heat developed during plastic extension of metals. Proc R Soc A 107:422–451

Hartley KA, Duffy J, Hawley RH (1987) Measurement of the temperature profile during shear band formation in mild steels deforming at high-strain rates. J Mech Phys Solids 35:283–301

Heidenreich RD, Shockley W (1948) Geometry of dislocations. In: Bristol conference on strength of solids. R Phys Soc Lond, Bristol

Hines JA, Vecchio KS (1997) Recrystallization kinetics within adiabatic shear bands. Acta Mater 45:635–649

Hirth JP, Lothe J (1968) Theory of dislocations. McGraw-Hill, New York

Hodowany J, Ravichandran G, Rosakis AJ, Rosakis P (2000) Partition of plastic work into heat and stored energy in metals. Exp Mech 40:113–123

Hosseini E, Kazeminezhad M (2009) ETMB model investigation of flow softening during severe plastic deformation. Comput Mater Sci 46:902–905

Kocks UF (1976) Laws for work hardening and low-temperature creep. J Eng Mater Technol 98:76–85

Kubin LP (1993) Dislocation patterning. In: Mughrabi H (ed) Materials science and technology, vol 6. VCH Verlagsgesellschaft, Weinheim, pp 137–190

Liao SC, Duffy J (1998) Adiabatic shear band in a Ti-6Al-4V titanium alloy. J Mech Phys Solids 46:2201–2231

Marchand A, Duffy J (1988) An experimental study of the formation process of adiabatic shear bands in a structural steel. J Mech Phys Solids 36:251–283

Merzer AM (1982) Modelling of adiabatic shear band development from small imperfections. J Mech Phys Solids 30:323–328

Meyers MA (1994) Dynamic behavior of materials. Wiley, New York

Meyers MA, LaSalvia JC, Nesterenko VF, Chen YJ, Kad BK (1996) Dynamic recrystallization in high strain rate deformation. In: The third international conference on recrystallization and related phenomena, pp 279–286

Meyers MA, Nesterenko VF, LaSalvia JC, Xu YB, Xue Q (2000) Observation and modeling of dynamic recrystallization in high-strain, high strain-rate deformation of metals. J Phys IV France Colloq C3(PR9):51–56

Nes E (1998) Modelling of work hardening and stress saturation in FCC metals. Process Mater Sci 41:129–193

Orowan E (1948) Symposium on internal stresses in metals and alloys. Institute of Metals

Rittel D (1999) The conversion of plastic work to heat during high strain rate deformation of glassy polymers. Mech Mater 31:131–139

Rittel D, Landau P, Venkert A (2008) Dynamic recrystallization as a potential cause for adiabatic shear failure. Phys Rev Lett 101:165501

Rittel D, Wang ZG (2008) Thermo-mechanical aspects of adiabatic shear failure of AM50 and Ti6Al4V alloys. Mech Mater 40:629–635

Rittel D, Wang ZG, Merzer M (2006) Adiabatic shear failure and dynamic stored energy of cold work. Phys Rev Lett 96:075502

Taylor GI, Quinney H (1934) The latent energy remaining in a metal after cold working. Proc R Soc Lond 143:307–326

Tresca H (1879) Sur la fluidité et l'écoulement des corps solides. Annales du Conservatoire des Arts et Métiers 4

Zener C, Hollomon JH (1944) Effect of strain rate upon plastic flow of steel. J Appl Phys 15:22–32